Observational Study

Medicine

OPEN

An ^{18F}-FDG PET/CT-based radiomics nomogram for predicting progression-free survival in nasopharyngeal carcinoma

A retrospective cohort study

Jianpeng Lin, BS[a,b], Jinghua Liu, MSc[c,d], Yanli Liu, MSc[a], Zhendong Cao, MSc[e], Dong Wen, PhD[f], Yanjun Wu, PhD[a,b], Zhongxiao Wang, PhD[a,b], Xiaolei Zhang, PhD[a], Bingzhen Wang, MSc[a,b], Shuyan Li, MSc[g], Xianling Dong, PhD[a,b,*]

Abstract

This study aimed to develop and validate a positron emission tomography/computed tomography (PET/CT)-based nomogram for individualized prediction of 3-year progression-free survival (PFS) in patients with nasopharyngeal carcinoma (NPC). A total of 128 patients with NPC who underwent pretreatment PET/CT imaging were retrospectively enrolled. Radiomic features were extracted from PET and CT images, and clinical variables were collected. Feature selection was performed using univariate Cox analysis, multivariable Cox analysis, and the least absolute shrinkage and selection operator regression to identify independent predictors. A nomogram was constructed by integrating CT-Radscore, PET-Radscore, and key clinical variables. Model performance in predicting 3-year PFS was evaluated using the concordance index, time-dependent area under the receiver operating characteristic curve, Kaplan–Meier survival curves, calibration curves, and decision curve analysis in both training and validation cohorts. The nomogram incorporating CT-Radscore, PET-Radscore, and lactate dehydrogenase demonstrated robust predictive ability for PFS in NPC. The area under the receiver operating characteristic curve for predicting 3-year PFS was 0.813 in the training cohort and 0.739 in the validation cohort. The corresponding concordance index values were 0.705 and 0.635, respectively. Calibration plots and decision curve analysis confirmed the nomogram's reliability and clinical utility. A PET/CT-based radiomics nomogram (CT-Radscore, PET-Radscore, and lactate dehydrogenase) achieved robust prediction of 3-year PFS and enhanced prognostic stratification in NPC. External validation in larger multi-center cohorts is needed due to the single-center retrospective design and moderate sample size.

Abbreviations: ^{18F}-FDG = ^{18F}-fluorodeoxyglucose, AUC = area under the curve, CI = confidence interval, C-index = concordance index, CT = computed tomography, DCA = decision curve analysis, LASSO = least absolute shrinkage and selection operator, LDH = lactate dehydrogenase, NPC = nasopharyngeal carcinoma, PET = positron emission tomography, PFS = progression-free survival.

Keywords: nasopharyngeal carcinoma, nomogram, PET/CT, survival analysis

JL and JL have contributed equally to this work.

This work was supported by Hebei Province Introduced Returned Overseas Chinese Scholars Funding Project (C20220107), and Hebei Province Higher Education Teaching Reform Research and Practice Project (2023GJJG322), Chengde Biomedicine Industry Research Institute Funding project (202205B086), and Chengde Medical University Project (202307, 202404).

The authors have no conflicts of interest to disclose.

The datasets generated during and/or analyzed during the current study are not publicly available, but are available from the corresponding author on reasonable request.

The study was approved by the Ethics Committee of Nanfang Hospital of Southern Medical University. All procedures involving human participants were performed according to the ethical standards of the institutional and/or national research committee and with the 1964 Helsinki declaration and its later amendments or comparable ethical standards. Informed consent was waived due to the nature of the retrospective study.

Supplemental Digital Content is available for this article.

[a] Hebei International Research Center for Medical-Engineering, Chengde Medical University, Hebei, China, [b] Hebei Key Laboratory of Nerve Injury and Repair, Chengde Medical University, Hebei, China, [c] Department of Nursing, Chengde Central Hospital, Chengde City, Hebei Province, China, [d] Department of Nursing, Faculty of Medicine and Health Sciences, University Putra Malaysia, Serdang, Malaysia, [e] Department of Radiology, The Affiliated Hospital of Chengde Medical University, Chengde, Hebei, China, [f] Institute of Artificial Intelligence, University of Science and Technology Beijing, Beijing, China, [g] Tianjin Corps Hospital of Chinese Armed Police Force, Tianjin, China.

** Correspondence: Xianling Dong, Hebei International Research Center for Medical-Engineering, Chengde Medical University, Chengde 067000, Hebei, China (e-mail: dongxl@cdmc.edu.cn).*

How to cite this article: Lin J, Liu J, Liu Y, Cao Z, Wen D, Wu Y, Wang Z, Zhang X, Wang B, Li S, Dong X. An ^{18F}-FDG PET/CT-based radiomics nomogram for predicting progression-free survival in nasopharyngeal carcinoma: A retrospective cohort study. Medicine 2026;105:7(e47716).

Received: 5 October 2025 / Received in final form: 30 December 2025 / Accepted: 28 January 2026

http://dx.doi.org/10.1097/MD.0000000000047716

1. Introduction

Nasopharyngeal carcinoma (NPC) is a head-and-neck malignancy that occurs predominantly in East and Southeast Asia, reaching ~30 per 100,000 in southern China.[1–3] Although intensity-modulated radiotherapy has markedly improved locoregional control and overall survival, disease progression and distant failure still occur in a substantial subset of patients.[4] In clinical practice, early identification of high-risk patients enables the timely intensification of therapy, such as the addition of induction chemotherapy or the inclusion of immunotherapy in treatment protocols. Conversely, accurate prediction of low-risk cases may allow for de-intensification strategies to reduce long-term toxicities without compromising disease control. Therefore, robust and individualized tools for progression-free survival (PFS) prediction are essential for personalized treatment planning in NPC. Risk stratification in routine practice continues to rely chiefly on the tumor node metastasis staging system.[5] However, tumor node metastasis stages have been confirmed as independent prognostic indicators,[6–8] they fail to capture the full spatial and biological heterogeneity of NPC, resulting in heterogeneous outcomes among patients within the same stage or biomarker category. Consequently, more accurate, individualized prognostic tools are required to guide treatment escalation or de-escalation and to improve long-term outcomes.[9]

Radiomics converts standard medical images into quantitative features to characterize tumor heterogeneity non-invasively, showing promise for oncological decision support.[10–12] These features: including intensity statistics, shape descriptors, and texture metrics: capture spatial patterns that correlate with underlying biological processes such as hypoxia, angiogenesis, and proliferation.[10,13] In NPC, ^{18F}-fluorodeoxyglucose (^{18F}-FDG) positron emission tomography/computed tomography (PET/CT) is routinely used for diagnosis, staging, and post-treatment surveillance.[14,15] Both conventional metrics (e.g., metabolic tumor volume) and advanced radiomic features derived from PET and CT have demonstrated prognostic value; for example, Huang et al demonstrated that radiomic features extracted from pretreatment CT images achieved superior prognostic performance for PFS in advanced-stage NPC patients.[16] Kim et al evaluated radiomic features extracted from pretreatment FDG PET images in patients with NPC, and demonstrated that models based on these features achieved predictive performance for PFS comparable to or better than those based on conventional PET parameters and clinical variables.[17] However, most existing studies have focused on a single imaging modality or employed simplistic pre-/post-treatment comparisons, thereby overlooking the potential synergistic value of integrating multi-modal imaging signatures with clinical biomarkers.[18–20] Notably, Lv et al reported that combining PET and CT radiomics outperformed either modality alone for survival prediction,[21] while Kim et al showed that both baseline and delta PET features correlated with outcomes.[17] Nevertheless, the potential complementary power of integrating multi-modal imaging signatures with established clinical biomarkers has been underexplored. Addressing this gap could yield a more comprehensive and robust prognostic model capable of refining risk stratification and guiding personalized management in NPC.

This retrospective study aimed to develop and validate a prognostic nomogram integrating PET/CT-derived radiomic signatures (Radscore) and key clinical variables to predict 3-year PFS in patients with NPC.

2. Methods

2.1. Study design and patient population

This study was a single-center retrospective observational cohort study conducted at the Nanfang Hospital of Southern Medical University, approved by the Ethics Committee of Nanfang Hospital of Southern Medical University, and included patients with histologically confirmed NPC between January 2012 and August 2016. The requirement for informed consent was waived due to the retrospective nature of the study. Clinical and laboratory data were retrospectively collected from the hospital information system. The extracted variables included demographic characteristics (age, sex), tumor classification (T-stage, N-stage, M stage, and clinical stage), treatment information (radiotherapy, chemotherapy), histopathological subtype, and Epstein–Barr virus serological markers, including immunoglobulin A antibodies. In addition, peripheral blood biomarkers were recorded, including lymphocyte count, neutrophil count, hemoglobin level, platelet count, and lactate dehydrogenase (LDH). PFS was defined as the time from the date of initial diagnosis to the 1st occurrence of disease progression/recurrence or death from any cause. Patients without an event were censored at the date of the last follow-up. The outcome status at the end of follow-up was recorded for each patient. To ensure data quality for subsequent modeling, patients with missing critical data (including incomplete clinical variables, laboratory values, or follow-up information) were excluded from the analysis. No imputation methods were applied to preserve the integrity of the dataset. Regarding model adequacy, although no formal power calculation was performed prospectively, the sample size (n = 128, with 68 events) exceeded the commonly recommended ratio of 10 events per predictor variable for survival models.[22,23] The final nomogram included 3 predictors, resulting in an events per predictor variable of 22.7, which is considered adequate for Cox proportional hazards regression. The 3-year PFS was selected as the primary endpoint, as most recurrences of nasopharyngeal carcinoma (NPC) occur within 3 years after treatment, and the median follow-up duration allowed sufficient assessment of this outcome.

2.2. Image acquisition

2.2.1. ^{18F}-FDG PET/CT protocol. All patients underwent pretreatment whole-body ^{18F}-FDG PET/CT imaging following the European Association of Nuclear Medicine guidelines.[24] The scans were performed using a Biograph mCT-128 PET/CT system (Siemens Healthineers, Shenzhen, China). Patients were required to fast for at least 6 hours before intravenous administration of ^{18F}-FDG (mean dose: 387 ± 41 MBq, range: 306–468 MBq; approximately 5.5 MBq/kg of body weight). After an uptake period of approximately 60 minutes (mean: 58 ± 5 min), PET/CT scans were acquired with the patients in a supine position to minimize motion artifacts. The CT acquisition parameters were set at 120 kVp and 80 mA, and CT images were used for attenuation correction. PET images were reconstructed using ordered-subset expectation maximization with 3 iterations and 21 subsets. The initial reconstruction matrix size for PET was 200 × 200 with a voxel size of 4.07 × 4.07 × 5.00 mm^3.

2.2.2. Multimodal image co-registration. PET images were resampled to match the CT spatial resolution (matrix: 512 × 512; voxel size: 0.98 × 0.98 × 3.00 mm^3) using cubic interpolation, thereby facilitating precise image co-registration and integrated multi-modal analysis. Cubic interpolation was employed as it optimally balances image quality preservation and computational efficiency while minimizing resampling-induced artifacts, which is essential for maintaining the fidelity of quantitative imaging features in radiomics analysis. The resulting preprocessed PET and CT images were subsequently utilized for tumor segmentation and radiomics feature extraction.

2.3. Radiomics analysis

2.3.1. Tumor segmentation. Tumor segmentation was independently performed by 2 experienced radiologists using ITK-SNAP software (version 3.4, www.itksnap.org), primarily based on the co-registered PET/CT images. To evaluate the consistency between observers, the Sorensen–Dice similarity coefficient was calculated for the delineated tumor volumes. The mean DSC was 0.86 ± 0.07, indicating good agreement between observers. For cases with DSC < 0.75, the 2 radiologists jointly reviewed the segmentations and reached consensus through discussion. The final agreed-upon segmentations were used for subsequent radiomics analysis.

2.3.2. Image preprocessing. Preprocessing of PET and CT images before feature extraction involved several steps. The images were 1st resampled to a voxel size of $1 \times 1 \times 1\,mm^3$ through linear interpolation to standardize voxel spacing. Subsequently, all PET and CT images were resized to a uniform matrix size of $80 \times 80 \times 64$ voxels to standardize input dimensions for downstream analysis. Finally, each image volume was cropped along the tumor boundaries defined by the corresponding manually annotated masks using SimpleITK, thereby retaining only the tumor-containing region of interest for radiomics feature extraction.

2.3.3. Radiomics feature extraction. Radiomics features were extracted from the preprocessed PET and CT images using the open-source PyRadiomics package (version 3.0.1)[25] implemented in Python (version 3.9.13; Python Software Foundation, Wilmington). Tumor regions were defined based on the manually delineated segmentation masks obtained from co-registered PET/CT images. A total of 1834 radiomics features were extracted from each imaging modality, including shape-based features, 1st-order intensity statistics, and texture features derived from the gray-level co-occurrence matrix, gray-level run-length matrix, gray-level size zone matrix, gray-level dependence matrix, and neighboring gray tone difference matrix.

2.4. Model development

2.4.1. Radiomics feature selection. To ensure the robustness and interpretability of radiomics features, a 3-step selection process was applied independently for CT and PET modalities. First, all extracted features were standardized using *z*-score normalization to eliminate scale differences. Then, univariate Cox proportional hazards regression was performed to identify features significantly associated with PFS. Subsequently, a least absolute shrinkage and selection operator (LASSO) Cox regression model[26] was implemented to further reduce dimensionality and select the most prognostic features within each modality. Based on the final selected features, modality-specific Radscore were calculated by linearly combining the features weighted by their corresponding LASSO-derived coefficients.

2.4.2. Clinical variable selection. For clinical variables, univariate Cox proportional hazards regression was performed to evaluate their association with PFS. Variables with a *P*-value < .05 in the univariate analysis were subsequently included in a multivariate Cox regression model. Stepwise model selection based on the Akaike Information Criterion was applied to identify independent prognostic factors. The selected clinical variables were then used for model construction and performance comparison with radiomics-based models.

2.4.3. Nomogram construction. A multivariable Cox proportional hazards model was developed to construct a radiomics-based nomogram, integrating the CT- and PET-derived radiomics signatures along with independent clinical predictors identified from univariate and multivariate analysis. The nomogram was built to estimate individualized probabilities of PFS.

2.4.4. Model evaluation and performance assessment. Model performance was evaluated using multiple complementary metrics. The concordance index (C-index) was calculated to assess the overall discriminative ability of the models for predicting PFS. Time-dependent receiver operating characteristic curves were generated, and the area under the curve (AUC) was calculated to evaluate predictive accuracy at the 3-year time point.

For risk stratification analysis, patients were dichotomized into high-risk and low-risk groups based on the median value of the combined radiomics score in the training cohort. The median cutoff was selected to ensure balanced group sizes and adequate statistical power for survival comparisons, to maintain clinical interpretability consistent with common practice in radiomics-based prognostic studies, and to reduce the risk of overfitting compared with data-driven cutoff optimization methods, such as maximally selected rank statistics. Kaplan–Meier survival curves were constructed for each risk group, and differences in PFS were assessed using the log-rank test.

Calibration curves were plotted to visually evaluate the agreement between nomogram-predicted probabilities and observed frequencies of 3-year PFS. Decision curve analysis (DCA) was performed to assess the clinical utility of the nomogram by quantifying the net benefit across different threshold probabilities, compared with strategies of treating all patients or treating none.

2.5. Statistical analysis

All statistical analyses were conducted using R software (version 4.2.1; R Foundation for Statistical Computing, Vienna, Austria). Continuous variables were summarized as mean ± standard deviation or median with interquartile range, depending on their distribution assessed by the Shapiro–Wilk test. Categorical variables were presented as frequencies and percentages. Group comparisons were performed using the Student *t* test or Mann–Whitney *U* test for continuous variables, and the chi-square test or Fisher exact test for categorical variables.

Univariate Cox proportional hazards regression was used to identify variables associated with PFS, followed by multivariate Cox regression to determine independent prognostic factors. Variables with a *P*-value < .05 were further analyzed using LASSO regression for dimensionality reduction and feature selection. Significant predictors were then included in a multivariable Cox regression model to construct the nomogram using the "rms" package in R.

A 2-sided *P*-value < .05 was considered statistically significant. We used the Strengthening the Reporting of Observational Studies in Epidemiology reporting guideline[27] to draft this manuscript, and the Strengthening the Reporting of Observational Studies in Epidemiology reporting checklist when editing, included in Table S1, Supplemental Digital Content, https://links.lww.com/MD/R381.

3. Results

3.1. Patient characteristics

This study included 128 patients with NPC, comprising 103 males and 25 females, who were randomly divided into a training cohort (n = 85) and a validation cohort (n = 43). The clinical characteristics of the 2 cohorts are presented in Table 1.

There were no statistically significant differences between the cohorts in terms of age, sex, American Joint Committee on Cancer stage, pathological subtype, receipt of radiotherapy or chemotherapy, VCA-immunoglobulin A, serum biochemical

Table 1

Clinical and demographic information of the 2 cohorts.

Characteristic	Training cohort	Validation cohort	*P*-value
No. of patients	85 (66%)	43 (34%)	
Age (yr)			
Median (range)	47 (15–78)	49 (21–74)	
Mean ± SD	47.5 ± 13.3	48.2 ± 13.2	.78
Gender			
Male	67 (78.8%)	36 (83.7%)	
Female	18 (21.2%)	7 (16.3%)	.639
AJCC stage			
I	2 (2.4%)	2 (4.7%)	
II	8 (9.4%)	3 (6.9%)	
III	33 (38.8%)	16 (37.2%)	
IV	42 (49.4%)	22 (51.2%)	.869
Radiotherapy (yes)	65 (76.5%)	33 (76.7%)	.972
Chemotherapy (yes)	69 (81.2%)	37 (86.0%)	.49
Pathology			
Non-keratinizing carcinoma	69 (81.2%)	38 (88.4%)	
Keratinizing squamous cell carcinoma	16 (18.8%)	5 (11.6%)	.449
VCA-IgA positive	53 (62.4%)	22 (51.2%)	.225
EB virus copies/mL			
Median (range)	500 (500–43,900)	896 (500–138,000)	
Mean ± SD	20,137 ± 61,263	81,586 ± 267,120	.045
LYM (G/L)			
Median (range)	1.64 (0.66–3.9)	1.79 (0.52–6.17)	
Mean ± SD	1.80 ± 0.67	2.02 ± 1.11	.157
NEU (G/L)			
Median (range)	4.35 (1.78–16.97)	4.09 (2.31–10.72)	
Mean ± SD	4.86 ± 2.17	4.78 ± 1.88	.849
HGB (g/L)			
Median (range)	142 (87–182)	141 (99–175)	
Mean ± SD	140.1 ± 18.14	139.0 ± 16.9	.753
PLT (G/L)			
Median (range)	251 (97–528)	246 (139–389)	
Mean ± SD	261.3 ± 223.4	252.6 ± 53.8	.624
LDH (U/L)			
Median (range)	166.6 (104–2088)	175 (110–1575.8)	.343
PFS (months)			
Median (range)	22 (1–56)	25 (4–52)	
Mean ± SD	23.7 ± 13.8	24.4 ± 14.0	.781
Event status			.847
Event	45 (52.9%)	23 (53.5%)	
Censored	40 (47.1%)	20 (46.5%)	

AJCC = American Joint Committee on Cancer, EB = Epstein–Barr virus, HGB = hemoglobin, IgA = immunoglobulin A, LDH = lactate dehydrogenase, LYM = lymphocyte, NEU = neutrophil, PFS = progression-free survival, PLT = platelet.

indicators, or follow-up duration (all *P*-values ranging from .157–.972), except for Epstein–Barr virus status ($P = .045$).

The median PFS was 22 months (range: 1–56 months) in the training cohort and 25 months (range: 4–52 months) in the validation cohort. At the last follow-up, 9 deaths, 19 local recurrences, and 12 distant metastases were recorded in the training cohort, whereas 6 deaths, 9 recurrences, and 5 metastases occurred in the validation cohort.

3.2. Feature selection and Radscore construction

A total of 1834 CT-based and 1834 PET-based features were initially extracted. Subsequently, a total of 398 CT-derived and 325 PET-derived radiomic features were identified as significantly associated with PFS based on univariate Cox analysis.

To further reduce dimensionality and address potential collinearity, LASSO Cox regression with 5-fold cross-validation was applied within each modality. As a result, 5 CT features and 6 PET features with non-zero coefficients were selected. The final Radscores were calculated as linear combinations of the selected features weighted by their corresponding LASSO-derived coefficients. These modality-specific Radscores were subsequently used as continuous variables for survival analysis and integration with clinical predictors. The selected features and their corresponding coefficients are detailed in Table 2.

3.3. Model establishment and validation

Univariate Cox regression analysis was performed in the training cohort to assess the prognostic relevance of clinical variables and radiomics signatures (CT-Radscore and PET-Radscore) to PFS. As summarized in Table 3, CT-Radscore ($P = .003$), PET-Radscore ($P < .001$), and LDH ($P = .024$) were significantly associated with PFS. No other clinical or laboratory parameters reached statistical significance ($P > .05$).

In the subsequent multivariable Cox regression analysis, CT-Radscore ($P = .028$), PET-Radscore ($P = .019$), and LDH ($P = .024$) remained statistically significant ($P < .05$), confirming their roles as independent prognostic factors. Notably, although T-stage demonstrated significance in the univariate analysis, it lost significance in the multivariate model, potentially due to confounding effects or collinearity with the imaging-derived variables.

Based on these findings, 4 prognostic models were constructed: a clinical model incorporating LDH; a CT model using CT-Radscore; a PET model using PET-Radscore; and

a nomogram model integrating all 3 significant predictors. A nomogram was generated to visualize this integrated model and facilitate individualized prediction of 3-year PFS.

Model performance was evaluated using C-index and AUC for 3 years in both the training and validation cohorts. As shown in Table 4, the nomogram model demonstrated the best performance, achieving a C-index of 0.705 (95% confidence interval [CI]: 0.698–0.711) and a 3-year AUC of 0.813 (95% CI: 0.809–0.826) in the training cohort. In the validation cohort, it maintained good discriminative ability, with a C-index of 0.635 (95% CI: 0.624–0.646) and AUC of 0.739 (95% CI: 0.717–0.750). The PET model showed moderate performance (train: C-index 0.671, AUC 0.721; validation: C-index 0.580, AUC 0.646), followed by the CT model (train: 0.617, 0.656; validation: 0.537, 0.651), while the clinical model exhibited the lowest predictive performance across both cohorts. Time-dependent receiver operating characteristic curves for all models are presented in Figure 1.

To further assess the prognostic stratification ability of each model, Kaplan–Meier survival analysis was performed by dichotomizing patients into high- and low-risk groups based on the median predicted risk score. As illustrated in Figure 2, the Nomogram model achieved the most distinct separation of survival curves in both cohorts, with statistically significant differences in the training ($P < .001$) and validation cohorts ($P = .013$). The Clinical model showed significant stratification in the validation cohort ($P = .03$) but not in the training cohort ($P = .15$). The PET model yielded borderline significance in the training cohort ($P = .14$) but was not significant in the validation cohort ($P = .26$). The CT model did not reach statistical significance in either cohort. These findings suggest that the integrated Nomogram model provides superior risk stratification and prognostic utility compared with single-modality models.

Table 2

Selected radiomics features.

CT radiomics features	Coef
Original_glszm_SmallAreaEmphasis	-0.052472269
Wavelet.HLL_firstorder_Mean	-0.060776689
Exponential_firstorder_Uniformity	0.037922119
Exponential_glcm_MaximumProbability	0.05238679
Exponential_glszm_LowGrayLevelZoneEmphasis	-0.005742124
PET radiomics features	
Wavelet.LHH_glcm_Correlation	-0.132200669
Wavelet.HLL_ngtdm_Contrast	0.027424867
Wavelet.HHL_ngtdm_Contrast	0.027424867
Wavelet.HHH_firstorder_Mean	-0.058933654
Wavelet.HHH_glcm_Idn	-0.058933654
Wavelet.HHH_ngtdm_Contrast	0.038405501

CT = computed tomography, PET = positron emission tomography.

3.4. Establishment and validation of the nomogram

Based on the multivariate Cox regression analysis, a prognostic nomogram was developed to provide an individualized estimation of 3-year PFS. The nomogram incorporated 3 independent predictors: CT-Radscore, PET-Radscore, and LDH. As shown in Figure 3, each predictor was assigned a point value proportional to its contribution to the outcome. The total score, calculated by summing the individual points, was mapped to the bottom scale to estimate the probability of 3-year PFS. This visualization

Table 3

Univariable Cox regression analysis of clinical variables for PFS.

	Univariate		Multivariate	
Variables	**HR (95% CI)**	***P*-value**	**HR (95% CI)**	***P*-value**
Age	1.00 (0.98–1.02)	.857		
Gender				
Male	Reference			
Female	0.97 (0.55–1.73)	.93		
T-stage			1.16 (1.12–1.49)	.26
T1	Reference			
T2	2.58 (1.13–5.91)	.025		
T3	1.41 (0.69–2.86)	.343		
T4	1.50 (0.66–3.40)	.328		
N-stage				
N0	Reference			
N1	2.11 (0.90–4.94)	.086		
N2	1.64 (0.74–3.63)	.226		
N3	1.85 (0.65–5.30)	.25		
Stage				
Stage 1	Reference			
Stage 2	2.73 (0.72–10.39)	.141		
Stage 3	1.17 (0.35–3.84)	.802		
Stage 4	1.19 (0.34–4.10)	.788		
IGA				
Negative	Reference			
Positive	0.65 (0.39–1.06)	.085		
LYM	1.07 (0.77–1.48)	.695		
NEU	1.07 (0.98–1.16)	.137		
HGB	1.00 (0.99–1.02)	.907		
PLT	1.00 (1.00–1.01)	.209		
LDH	0.53 (0.30–0.92)	.024	0.52 (0.3–0.91)	.024
EB	0.84 (0.72–0.99)	.032	0.86 (0.73–1.02)	.082
CT_Radscore	1.42 (1.12–1.80)	.003	1.30 (1.03–1.65)	.028
PET_Radscore	1.49 (1.21–1.83)	<.001	1.31 (1.04–1.65)	.019

CT = computed tomography, EB = Epstein–Barr virus, HGB = hemoglobin, IgA = immunoglobulin A, LDH = lactate dehydrogenase, LYM = lymphocyte, NEU = neutrophil, PET = positron emission tomography, PFS = progression-free survival, PLT = platelet.

Table 4

Performance comparison of different models in predicting 3-year PFS.

Model	C-index (training)	C-index (validation)	AUC@3y (training)	AUC@3y (validation)
Clinical model	0.580 (0.573–0.588)	0.619 (0.606–0.633)	0.687 (0.675–0.695)	0.648 (0.626–0.666)
CT model	0.617 (0.611–0.624)	0.537 (0.528–0.546)	0.656 (0.643–0.666)	0.651 (0.633–0.665)
PET model	0.671 (0.664–0.678)	0.580 (0.570–0.589)	0.721 (0.710–0.732)	0.646 (0.630–0.663)
Nomogram model	0.705 (0.698–0.711)	0.635 (0.624–0.646)	0.813 (0.809–0.826)	0.739 (0.717–0.750)

AUC = area under the curve, C-index = concordance index, CT = computed tomography, PET = positron emission tomography, PFS = progression-free survival.

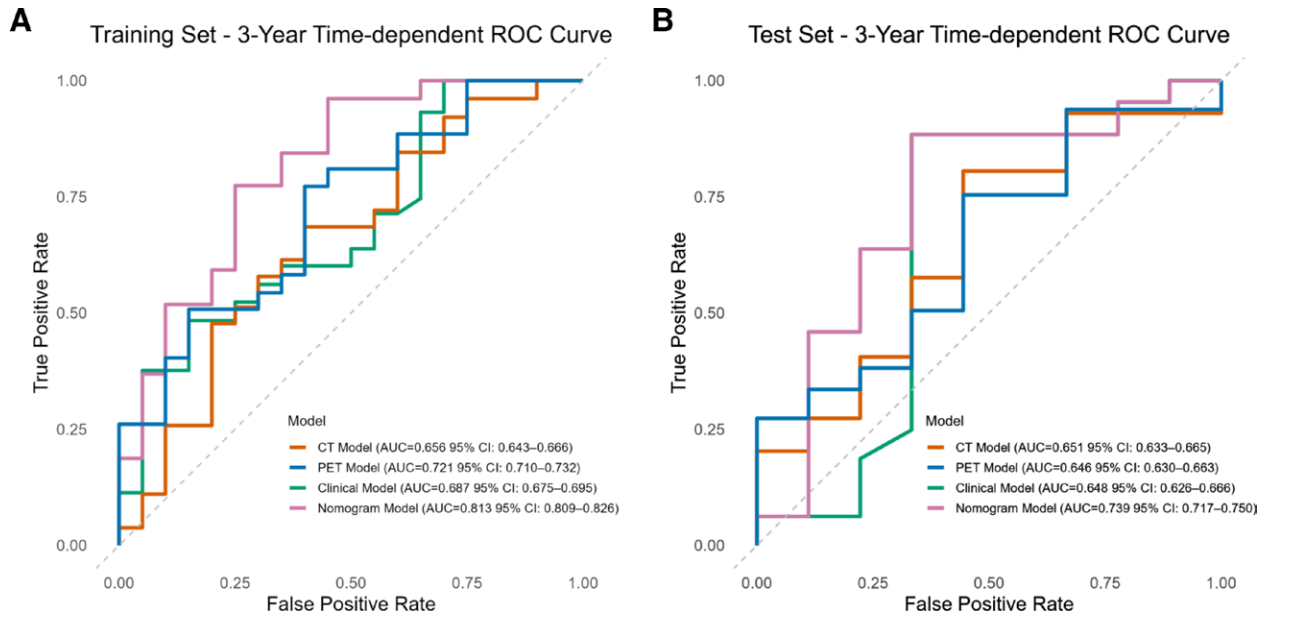

Figure 1. Time-dependent ROC curves of 4 models for predicting 3-year PFS in the training (A) and validation (B) cohorts. PFS = progression-free survival, ROC = receiver operating characteristic.

provides an intuitive and practical tool for clinical risk stratification and decision-making in patients with NPC.

To evaluate the accuracy of the nomogram in estimating individualized survival probabilities, calibration curves were generated in both the training and validation cohorts, as shown in Figure 4. In the training cohort (Fig. 4A), the calibration curve demonstrated a generally good agreement between the predicted and actual 3-year PFS probabilities. Most calibration points were located close to the ideal 45-degree reference line, indicating that the nomogram's predicted risk was well-aligned with the observed outcomes. However, in the lower predicted probability range (0.1–0.3), the model slightly overestimated the true PFS, as indicated by a mild downward deviation from the diagonal. The overall pattern remained consistent, and the confidence intervals overlapped with the reference line in most risk intervals, supporting the model's accuracy in the training data. In contrast, the validation cohort (Fig. 4B) showed a less smooth calibration curve with larger confidence intervals. The number of available risk intervals was lower, likely due to a smaller sample size and fewer events, which reduced the statistical stability of the estimates. Nonetheless, the predicted and observed survival probabilities followed a similar trend, and the curve remained reasonably close to the diagonal line. Despite the increased variability, the nomogram preserved a satisfactory level of calibration in the validation cohort, supporting its generalizability.

To further evaluate the clinical utility of the proposed model, DCA was conducted to assess the net benefit of the nomogram compared with individual modality-based models and the clinical model. As shown in Figure 5, the nomogram consistently demonstrated the highest net benefit across a broad range of threshold probabilities in both the training (Fig. 5A) and validation cohorts (Fig. 5B). In the training cohort, the nomogram showed clear superiority over all other models, particularly within the threshold probability range of 0.2 to 0.4, which is clinically relevant for risk-based decision-making. The net benefit of the nomogram remained well above the "treat-all" and "treat-none" strategies across almost the entire range, highlighting its enhanced ability to correctly identify patients who are more likely to experience disease progression. In the validation cohort, despite slightly reduced separation among the models, the nomogram continued to outperform the CT, PET, and clinical models, maintaining a robust clinical net benefit throughout most of the decision thresholds. This consistent advantage indicates that the nomogram not only achieves strong predictive accuracy but also delivers meaningful clinical value in real-world applications by optimizing individualized treatment strategies.

4. Discussion

In this study, we developed and validated a comprehensive prognostic nomogram that integrates radiomics features extracted from both CT and PET imaging modalities with key clinical parameters, including LDH, to provide individualized prediction of 3-year PFS in patients with NPC. Our approach involved rigorous feature selection and model construction: we 1st extracted a large number of quantitative radiomics features from segmented tumor regions on CT and PET images, and then applied univariate Cox regression, multivariate Cox regression, and LASSO-based multivariate selection to identify the most prognostically relevant features for each imaging modality. Our main finding is that the fusion model, which combines

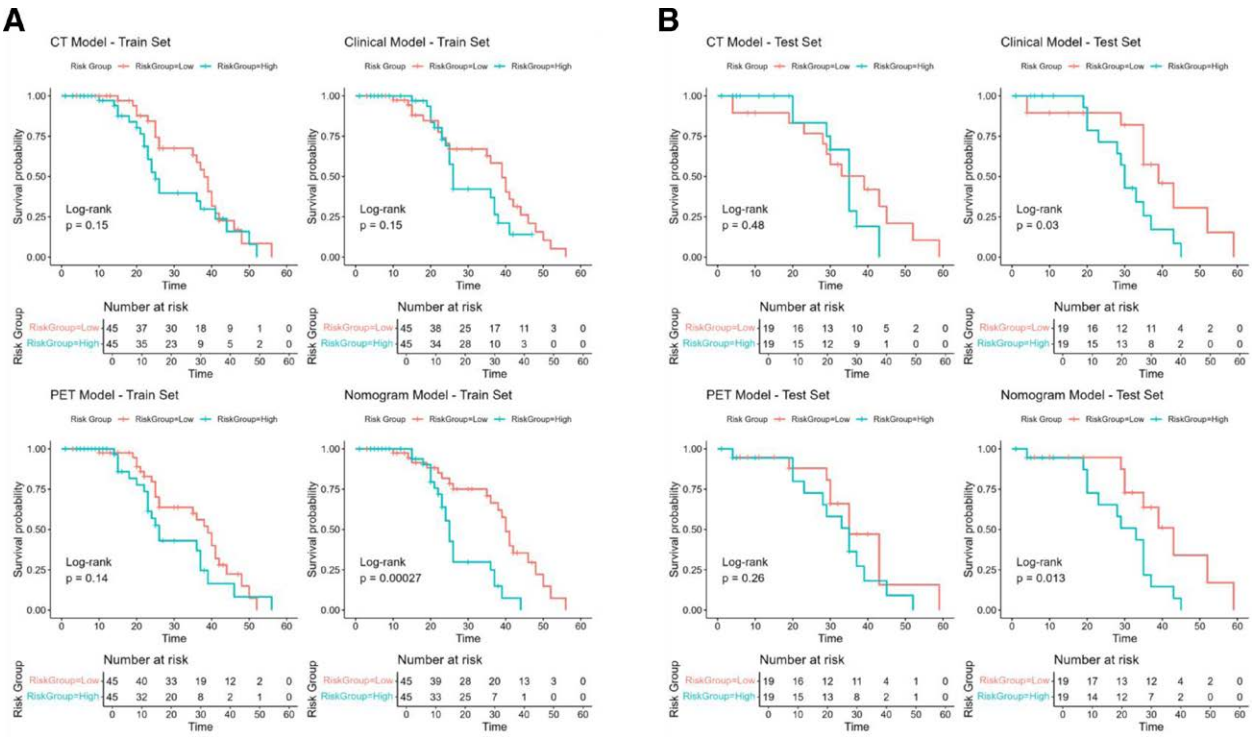

Figure 2. Kaplan–Meier curves of high-risk and low-risk groups for each model in the training (A) and validation (B) cohorts.

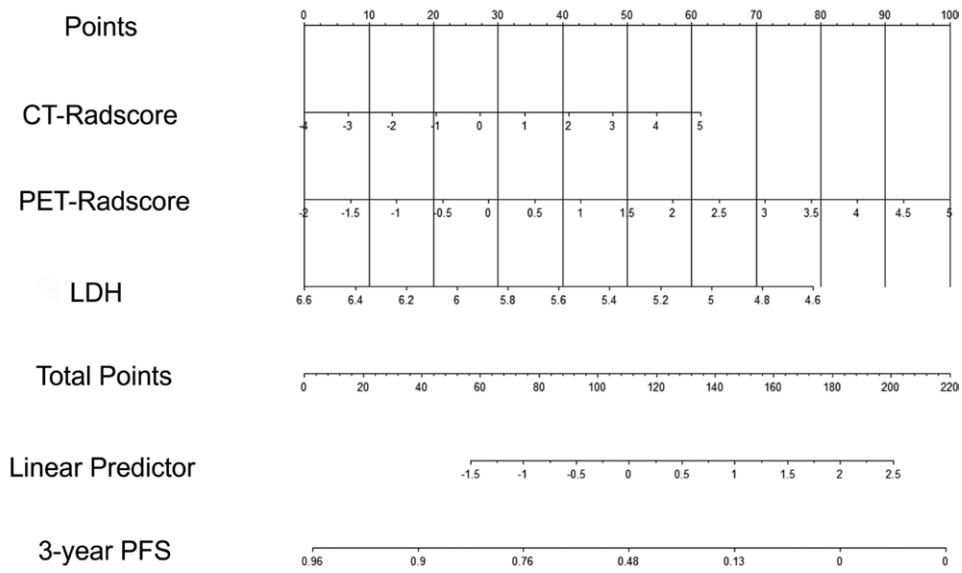

Figure 3. Nomogram for predicting PFS in NPC. NPC = nasopharyngeal carcinoma, PFS = progression-free survival.

multi-modalityradiomics and clinical features, consistently outperformed single-modality or clinical-only models in both the training and validation cohorts, demonstrating the value of a multidimensional approach for individualized risk assessment in NPC.

The results indicated that both CT- and PET-derived radiomics signatures were independent predictors of PFS, consistent with previous studies reporting associations between quantitative imaging features and clinical outcomes.[28–30] Notably, 3 previous studies have evaluated the prognostic performance of PET/CT-based radiomic features in NPC. In line with our findings, these studies reported that integrating clinical variables with PET/CT radiomic features improved PFS prediction, achieving C-index values of 0.77[21] and 0.69,[31] and an AUC of 0.829,[32] compared with a C-index of 0.705 and an AUC of 0.813 observed in our analysis. Compared to prior studies, our work demonstrates several distinct contributions. Peng et al[32] focused exclusively on advanced NPC (stages II–IV), while we included a broader patient population. In the study by Lv et al[21] no PET-derived radiomic features were retained in multivariable analysis. In contrast, our study successfully identified multiple significant CT- and PET-based radiomic features reflecting tumor heterogeneity, highlighting differences in radiomic signature selection across studies. Xu et al[31] incorporated only the American Joint Committee on Cancer stage as a clinical variable. By comparison,

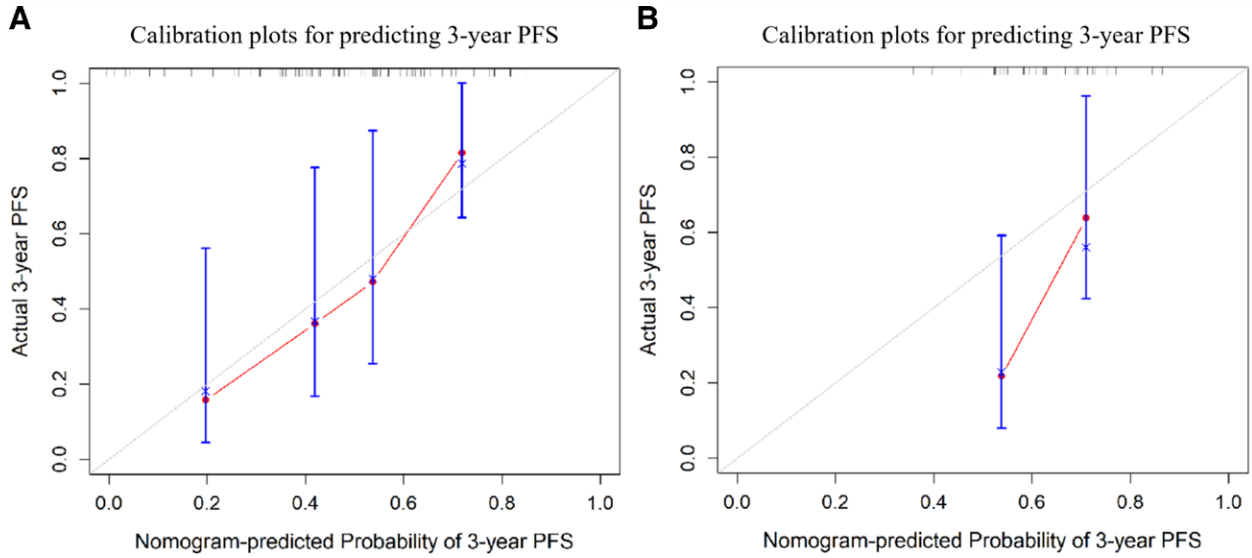

Figure 4. Calibration curves for the nomogram in predicting 3-year PFS in the training (A) and validation (B) cohorts. PFS = progression-free survival.

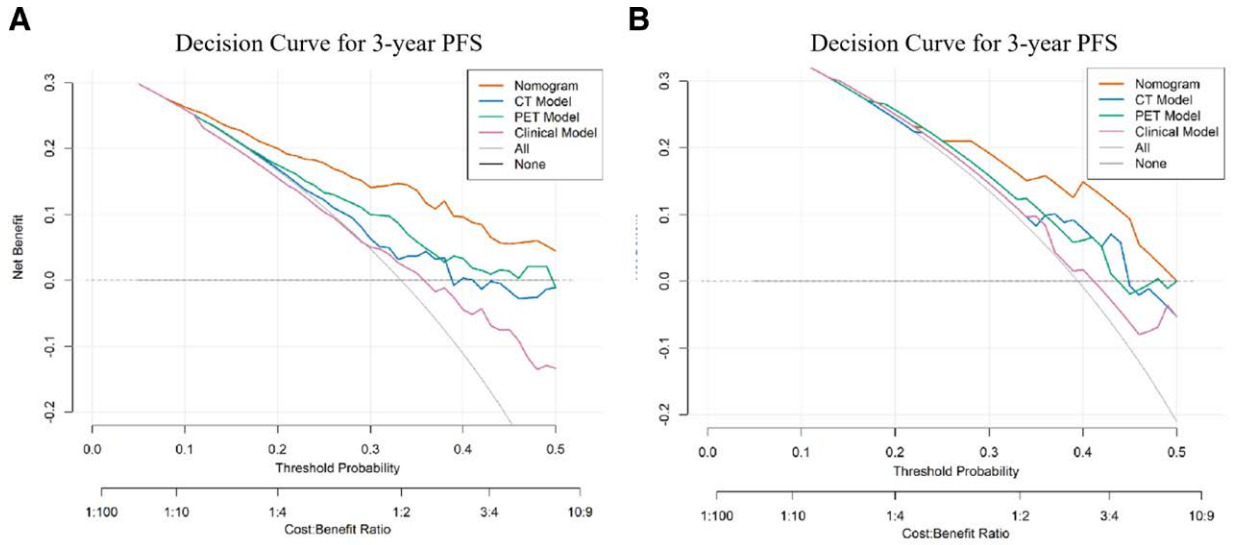

Figure 5. DCA for predicting 3-year PFS in the training (A) and validation (B) cohorts. DCA = decision curve analysis, PFS = progression-free survival.

our analysis identified LDH as an independent prognostic factor, suggesting biochemical markers may provide complementary value to conventional staging systems. Most importantly, none of these prior studies implemented a clinical nomogram for individualized risk prediction: a critical gap our study addresses. The nomogram was further validated by calibration curves and DCA, both of which demonstrated good agreement between predicted and observed outcomes and confirmed the model's clinical utility.

This study has several notable strengths. First, a multidimensional approach integrating CT- and PET-derived radiomics features with clinical biomarkers was developed. Second, a rigorous methodological framework, including internal validation and comprehensive performance evaluation, was applied to ensure reliable model assessment. Third, a clinically applicable nomogram was constructed to facilitate individualized risk stratification, which has not been extensively explored in previous radiomics studies of NPC. Despite these strengths, several important limitations should be acknowledged. The most critical limitation is the absence of external validation, which significantly restricts the generalizability of our findings. As a single-center retrospective study conducted at 1 institution, our results may not be directly applicable to other clinical settings with different patient populations, scanner protocols, or treatment approaches. Although we performed internal validation using a holdout test set, multi-center external validation is imperative to establish the reproducibility and clinical utility of our nomogram across diverse healthcare settings. Without such validation, the clinical implementation of our model remains premature. Second, we limited our survival prediction to the 3-year PFS endpoint as most NPC recurrences occur within this timeframe; future studies with extended follow-up are warranted to evaluate multiple time points (1-year and 5-year PFS). Third, radiomic reproducibility can be affected by variations in image acquisition protocols, reconstruction parameters, and segmentation methods. Harmonizing imaging protocols and establishing consensus-based feature extraction pipelines are essential for clinical translation. Finally, integrating other emerging biomarkers such as genomic, proteomic, or circulating tumor DNA markers may further enhance model performance.

Future research should prioritize multi-center prospective validation to confirm the generalizability and clinical utility of

our nomogram across diverse patient populations and imaging protocols. Additionally, extending prognostic modeling to include 1-year and 5-year PFS endpoints would provide a more comprehensive temporal risk assessment to guide personalized treatment strategies and surveillance planning. Integration of emerging biomarkers, including genomic and proteomic data, may further enhance predictive accuracy and clinical applicability.

5. Conclusion

In summary, our study demonstrates that the integration of CT and PET radiomics with clinical parameters such as LDH yields a robust and clinically meaningful tool for individualized prediction of 3-year PFS in NPC patients. The proposed nomogram exhibits superior prognostic performance, good calibration, and clear clinical benefit, highlighting its potential to guide risk-adapted treatment strategies and improve patient outcomes. With further validation and refinement, such multi-modal models may become an integral part of precision oncology for NPC.

Acknowledgments

We would like to thank Nanfang Hospital of Southern Medical University for support with clinical data collection and imaging database management. We also acknowledge the efforts of the clinicians, radiologists, and technical staff who contributed to patient care and data curation.

Author contributions

Conceptualization: Yanli Liu, Dong Wen.
Data curation: Jianpeng Lin, Jinghua Liu, Dong Wen, Bingzhen Wang, Shuyan Li.
Formal analysis: Jianpeng Lin, Zhongxiao Wang, Xiaolei Zhang.
Funding acquisition: Xianling Dong.
Investigation: Jianpeng Lin, Jinghua Liu, Xiaolei Zhang.
Methodology: Jianpeng Lin, Xiaolei Zhang, Xianling Dong.
Project administration: Jianpeng Lin.
Resources: Zhendong Cao, Shuyan Li.
Software: Jianpeng Lin, Zhendong Cao, Zhongxiao Wang, Bingzhen Wang, Shuyan Li.
Supervision: Yanjun Wu, Xianling Dong.
Validation: Jianpeng Lin, Yanjun Wu, Zhongxiao Wang, Shuyan Li.
Visualization: Jinghua Liu, Yanjun Wu, Bingzhen Wang.
Writing – original draft: Jianpeng Lin.
Writing – review & editing: Jianpeng Lin.

References

[1] Bray F, Laversanne M, Sung H, et al. Global cancer statistics 2022: GLOBOCAN estimates of incidence and mortality worldwide for 36 cancers in 185 countries. CA Cancer J Clin. 2024;74:229–63.
[2] Chen YP, Chan ATC, Le QT, Blanchard P, Sun Y, Ma J. Nasopharyngeal carcinoma. Lancet. 2019;394:64–80.
[3] Chua MLK, Wee JTS, Hui EP, Chan ATC. Nasopharyngeal carcinoma. Lancet. 2016;387:1012–24.
[4] Sun MX, Zhao MJ, Zhao LH, Jiang HR, Duan YX, Li G. A nomogram model based on pre-treatment and post-treatment MR imaging radiomics signatures: application to predict progression-free survival for nasopharyngeal carcinoma. Radiat Oncol. 2023;18:67.
[5] Zhang LL, Li YY, Hu J, et al. Proposal of a pretreatment nomogram for predicting local recurrence after intensity-modulated radiation therapy in t4 nasopharyngeal carcinoma: a retrospective review of 415 Chinese Patients. Cancer Res Treat. 2017;50:1084–95.
[6] Cho JK, Lee GJ, Yi KI, et al. Development and external validation of nomograms predictive of response to radiation therapy and overall survival in nasopharyngeal cancer patients. Eur J Cancer. 2015;51:1303–11.
[7] Tang LQ, Li CF, Li J, et al. Establishment and validation of prognostic nomograms for endemic nasopharyngeal carcinoma. J Natl Cancer Inst. 2016;108:djv291.
[8] Li J, Chen S, Peng S, et al. Prognostic nomogram for patients with Nasopharyngeal Carcinoma incorporating hematological biomarkers and clinical characteristics. Int J Biol Sci. 2018;14:549–56.
[9] Glastonbury CM, Salzman KL. Pitfalls in the staging of cancer of nasopharyngeal carcinoma. Neuroimaging Clin N Am. 2013;23:9–25.
[10] Gillies RJ, KinahCan PE, Hricak H. Radiomics: images are more than pictures, they are data. Radiology. 2016;278:563–77.
[11] Hatt M, Rest CCL, Tixier F, Badic B, Schick U, Visvikis D. Radiomics: data are also images. J Nucl Med. 2019;60(Supplement 2):38S–44S.
[12] Vallières M, Zwanenburg A, Badic B, Rest CCL, Visvikis D, Hatt M. Responsible radiomics research for faster clinical translation. J Nucl Med. 2018;59:189–93.
[13] Peng Z, Wang Y, Wang Y, et al. Application of radiomics and machine learning in head and neck cancers. Int J Biol Sci. 2021;17:475–86.
[14] Mohandas A, Marcus C, Kang H, et al. FDG PET/CT in the management of nasopharyngeal carcinoma. AJR Am J Roentgenol. 2014;203:W146–57.
[15] Gihbid A, Cherkaoui Salhi G, El Alami I, et al. Pretreatment [18F]FDG PET/CT and MRI in the prognosis of nasopharyngeal carcinoma. Ann Nucl Med. 2022;36:876–86.
[16] Huang YC, Huang SM, Yeh JH, et al. Utility of CT radiomics and delta radiomics for survival evaluation in locally advanced nasopharyngeal carcinoma with concurrent chemoradiotherapy. Diagnostics (Basel). 2024;14:941.
[17] Kim SJ, Choi JY, Ahn YC, Ahn MJ, Moon SH. The prognostic value of radiomic features from pre- and post-treatment 18F-FDG PET imaging in patients with nasopharyngeal carcinoma. Sci Rep. 2023;13:8462.
[18] Aprupe L, Litjens G, Brinker TJ, Laak J van der, Grabe N. Robust and accurate quantification of biomarkers of immune cells in lung cancermicro-environment using deep convolutional neural networks. PeerJ. 2019;7:e6335.
[19] Peng H, Dong D, Fang MJ, et al. Prognostic value of deep learning PET/CT-based radiomics: Potential role for future individual induction chemotherapy in advanced nasopharyngeal carcinoma. Clin Cancer Res. 2019;25:4271–9.
[20] Zhang LL, Huang MY, Li Y, et al. Pretreatment MRI radiomics analysis allows for reliable prediction of local recurrence in non-metastatic T4 nasopharyngeal carcinoma. eBioMedicine. 2019;42:270–80.
[21] Lv W, Yuan Q, Wang Q, et al. Radiomics analysis of PET and CT components of PET/CT imaging integrated with clinical parameters: application to prognosis for nasopharyngeal carcinoma. Mol Imaging Biol. 2019;21:954–64.
[22] Peduzzi P, Concato J, Kemper E, Holford TR, Feinstein AR. A simulation study of the number of events per variable in logistic regression analysis. J Clin Epidemiol. 1996;49:1373–9.
[23] Vittinghoff E, McCulloch CE. Relaxing the rule of ten events per variable in logistic and Cox regression. Am J Epidemiol. 2007;165:710–8.
[24] Boellaard R, Delgado-Bolton R, Oyen WJG, et al. FDG PET/CT: EANM procedure guidelines for tumour imaging: version 2.0. Eur J Nucl Med Mol Imaging. 2015;42:328–54.
[25] van Griethuysen JJM, Fedorov A, Parmar C, et al. Computational radiomics system to decode the radiographic phenotype. Cancer Res. 2017;77:e104–7.
[26] Tibshirani R. Regression shrinkage and selection via the lasso. J R Stat Soc Ser B Stat Methodol. 1996;58:267–88.
[27] Von Elm E, Altman DG, Egger M, Pocock SJ, Gøtzsche PC, Vandenbroucke JP. The Strengthening the Reporting of Observational Studies in Epidemiology (STROBE) statement: guidelines for reporting observational studies. Prev Med. 2007;45:247–51.
[28] Li H, Kong Z, Xiang Y, Zheng R, Liu S. The role of PET/CT in radiotherapy for nasopharyngeal carcinoma. Front Oncol. 2022;12:1017758.
[29] Ng SH, Chan SC, Yen TC, et al. Staging of untreated nasopharyngeal carcinoma with PET/CT: comparison with conventional imaging work-up. Eur J Nucl Med Mol Imaging. 2009;36:12–22.
[30] King AD, Ma BB, Yau YY, et al. The impact of 18F-FDG PET/CT on assessment of nasopharyngeal carcinoma at diagnosis. Br J Radiol. 2008;81:291–8.
[31] Xu H, Lv W, Feng H, et al. Subregional radiomics analysis of PET/CT imaging with intratumor partitioning: application to prognosis for nasopharyngeal carcinoma. Mol Imaging Biol. 2020;22:1414–26.
[32] Peng L, Hong X, Yuan Q, Lu L, Wang Q, Chen W. Prediction of local recurrence and distant metastasis using radiomics analysis of pretreatment nasopharyngeal [18F]FDG PET/CT images. Ann Nucl Med. 2021;35:458–68.